Performance and Scaling of a Dense Plasma Focus Light Source for EUV Lithography.

Igor V. Fomenkov, Richard M. Ness, Ian R. Oliver, Stephan T. Melnychuk, Oleh V. Khodykin, Norbert R. Böwering, Curtis L. Rettig, Jerzy R. Hoffman (Cymer, Inc. 16750 Via Del Campo Ct, San Diego, CA 92127).

A commercially viable light source for EUV lithography has to meet the large set of requirements of a High Volume Manufacturing (HVM) lithography tool. High optical output power, high-repetition rate, long component lifetime, good source stability, and low debris generation are among the most important parameters. The EUV source, being developed at Cymer, Inc. is a discharge produced plasma source in a dense plasma focus (DPF) configuration. Promising results with Xe as a working gas were demonstrated earlier. To scale the DPF parameters to levels required for HVM our efforts are concentrated on the following areas: (1) thermal engineering of the electrodes utilizing direct water cooling techniques; (2) development of improved pulsed power systems for > 4 kHz operation; (3) study of erosion mechanisms for plasma facing components; (4) development of efficient debris mitigation techniques and debris shields; (5) studies of plasma generation and evolution with emphasis on improving conversion efficiency and source stability; (6) development of EUV metrology techniques and instrumentation for measurements of source size; and (7) development of an optimized collector optic matched to our source parameters. In this paper, we will present results from each of these key areas. The total in-band EUV output energy now approaches 60 mJ/pulse into 2 π sr and the conversion efficiency has been increased to near 0.5 %. Routine operation at 4 kHz in burst-mode, and continuous operation at 1 kHz has been demonstrated. Improved at-wavelength source metrology now allows a determination of EUV source size utilizing imaging, and monitoring of key features of the spectrum on a pulse-to-pulse basis. With effective suppression of debris generated from the anode by several orders of magnitude, UV/EUV-catalyzed carbon growth now presents the limit in producing a clean source.

Keywords: EUV Lithography, EUV light source, Dense Plasma Focus, DPF, Plasma pinch, Xe emission.

1. INTRODUCTION

Extreme Ultraviolet (EUV) lithography systems designed for high volume manufacturing (HVM), which are planned to be introduced at the 32 nm node, will require sources of 13.5 nm radiation with extremely high power and brightness. We believe that discharge produced plasmas (DPP) can provide a cost effective scalable solution which can meet the requirements of commercial HVM tools. At Cymer, we have been developing a dense plasma focus (DPF) configuration as an EUV source. The DPF configuration provides an open geometry with large collection angle, operates over a wide range of gas pressures and flows, and can be scaled for high-repetition rate operation.

We believe that the thermal engineering and debris mitigation issues continue to pose the greatest technical risk toward achieving a production-worthy system. Over the past year our R&D efforts have been concentrated on: design and fabrication of high power plasma-facing electrodes; testing of insulator materials; development of metrology techniques; characterization of plasma, UV/EUV-induced debris and contamination; design of debris mitigation techniques; and upgrades of the pulsed power system.

All results presented in this paper have been obtained using our generation 4.0 pulse power system. The complete DPF system has been described in detail in previous publications[1-3].

Emerging Lithographic Technologies VII, Roxann L. Engelstad, Editor,
Proceedings of SPIE Vol. 5037 (2003) © 2003 SPIE · 0277-786X/03/$15.00

2. IN-BAND EUV ENERGY AND CONVERSION EFFICIENCY

The in-band EUV energy per pulse was measured using a diagnostic vessel equipped with a Mo-Si multi-layer mirror, two 0.2 μm Zr foils, and an un-coated IRD AXUV-100 photodiode. This system has been described in ref. [3]. Recent modifications to this diagnostic vessel include the addition of a flange with multiple ports allowing simultaneous measurement of in-band energy and EUV source images utilizing a pinhole camera. Data collection consists of recording all relevant system waveforms using a high-speed oscilloscope interfaced to a computer.

Figures 1 and 2 show the dependence of the 2% in-band energy, at 13.5 nm, and conversion efficiency (CE) on the energy dissipated in the discharge. The figures show the trend in CE over the past two years. The DPF configuration described in ref.[2] is taken as the baseline. Incremental improvements in the CE and energy per pulse have been achieved by improving the electrode geometry, the gas delivery system, the pre-ionization system, and most recently by modifications to the dynamics of the DPF plasma.

Modifications to the detailed electrode shapes have been driven largely by empirical knowledge gained from testing various configurations. We have observed scaling laws for the operating pressure of the DPF which depend on electrode and insulator details. The general trend in electrode geometry has been in the direction of larger diameter structures that are easier to cool at high-repetition rate operation. This has also resulted in a reduction in operating pressure of the machine. From the figures, we see that approximately an 85% improvement in CE at 10 J was achieved through a combination of modification to the gas recipe, the gas delivery system and the pre-ionization system.

Improvements in the pre-ionization electrodes have enabled us to explore a larger parameter space of the pre-ionization plasma. The use of an independently triggered pre-ionization system allows us to operate the DPF below the Paschen breakdown minimum. This type of DPF configuration in principle provides efficient matching of the DPF plasma load to the pulsed power system.

Recent modifications to the plasma driver have concentrated on configurations that provide some control of the plasma run-down and pinch phase independent of electrode structure. These latest improvements have resulted in a source capable of delivering 60 mJ per pulse corresponding to a CE of 0.45% at approximately 12 J of dissipated energy. Pulse-to-pulse root-mean-square (rms)energy stability for operation at low repetition rate is approx. 7%. The data also show that for this electrode configuration we have reached a plateau in the CE. Future improvements in the CE may require additional modifications to the electrode structure. In order to meet expected source performance specifications in terms of output power for HVM tools, we must increase our CE to at least 0.7%. Such systems could conceivably produce > 100W of collectable in-band EUV power.

At present, no sufficiently precise modeling codes exist in the public domain that can be used to predict in-band EUV output and DPF performance for realistic configurations operated with Xe as the active gas. Therefore, for the near future, improvements and modifications to machine performance will continue to be driven by empirical experimentation. Acknowledging the importance of the plasma dynamics on ultimate performance of the DPF as an EUV light source, we are collaborating with researchers at the University of Nevada, Reno, to model the plasma pinch and EUV emission. The plasma dynamics are simulated by the code MHRDR [8], a time-dependent radiation- magnetohydrodynamic code. Model derived quantities such as pinch timing, plasma kinetic energy, and density are being compared to experimentally measured parameters. In particular, the scaling of these quantities with geometric feature shapes and sizes are compared between code predictions and experimental measurements with the eventual objective for a predictive tool. Furthermore, a collisional-radiative plasma spectral model will be employed to predict the 13.5 nm light intensity and distribution that can also be compared with experimental measurements.

3. HIGH-REPETITION RATE OPERATION

High-repetition rate operation has been demonstrated on several of our DPF systems. Most recently, we have upgraded one DPF system with a 4kHz pulse power resonant charging system. This machine operates with an un-cooled electrode set. Burst-mode operation was carried out at low average power for bursts up to 1000 pulses at 2 kHz repetition rate, and 800 pulses at 4kHz. Burst length was limited by the temperature rise of the anode electrode. Figure 3 shows the normalized in-band EUV output at 2 kHz for a 1000 pulse. The rms variation in EUV in-band energy is 7%. Figure 4 shows similar data obtained at 4 kHz. The rms energy variation at 4 kHz was 9%. A characteristic [3] burst transient is seen in both figures. The initial pulses of the burst are low in EUV energy because the gas conditions are tuned to stabilize the EUV output at steady-state. Our experiments show that it is possible to optimize the EUV output at all repetition rates up to at least 4 kHz by adjustment of the gas recipe. The addition of cooling in the anode electrode is also expected to reduce the burst transient by maintaining a more constant gas density during the burst.

Thermal management, particularly for the electrodes, has long been viewed as one of the greater technical risks to the development of a production-worthy EUV light source for semiconductor lithography. Good progress has been made in the development of discharge region cooling over the last year and the path for further improvement is apparent.

Second generation direct water-cooled electrodes along with a first generation direct water-cooled vacuum vessel have been developed and tested. In addition, significant effort has been focused on the design of discharge region insulators. These new designs have resulted in a five-fold improvement in the maximum steady-state repetition rate over the last year from 200 Hz to 1000 Hz. Advanced electrode heat exchanger designs that provide extended cooling surfaces based on porous metal and micro-channels have also been developed. Testing of these using water as a coolant is scheduled in the near future.

Changes to the cathode, or outer electrode, to achieve 1000 Hz have been relatively minor, the existing design being largely able to support today's maximum steady-state repetition rate. On the contrary, the anode, or inner electrode, has changed significantly over the course of the last year. Much has been learned about the manufacturing techniques required to produce electrodes using refractory metals, such as molybdenum and tungsten, which present particular fabrication challenges. Use of such materials reduces the erosion rate of the anode considerably and lifetime of this component has been extended from a few million pulses to higher than 10 million pulses.

The development of joints between dissimilar metals for the electrodes with high structural and vacuum integrity has been successful. These developments have made important contributions to the ability to pump coolant safely through the device at high flow rates and pressures.

In a recent test, calorimetric data showed that 13 kW of heat was removed from the discharge region of the source. This was achieved with a flow rate of approximately 27 liters per minute and a delivery pressure in excess of 3400 kPa. As in some previous tests it was observed that more heat is removed from the anode, which is subjected to significantly higher heat flux per unit area, than from the cathode. The approximate distribution of heat removed from the discharge region at 1000 Hz was 50% from the anode, 40% from the cathode and 10% from the vacuum vessel.

Detailed finite element models of the anode have been created and good correlation between predicted performance and test data has been observed. Good correlation between the electrical energy input to the system and the heat removed has also been observed. It can be concluded from the analyses that the current generation of electrodes is capable of supporting significantly higher repetition rates than achieved thus far. This, and the active development of more advanced techniques for electrode cooling suggest that further work will yield further performance improvements.

4. SPECTRAL CHARACTERIZATION OF THE SOURCE

Spectral analysis of the emitted EUV radiation from the source is important in order to determine the partitioning of in-band and out-of-band EUV emission, mean electron temperature and spectral output stability under different operating conditions of the DPF. These characteristics will directly affect the source performance in terms of output power and dose stability. Most of the EUV emission of our source occurs in the region of 10 nm to 20 nm. The EUV spectrum of xenon consists of many overlapping lines and transition arrays that are generally not or only partially resolved. Spectra measured with higher resolution using a grazing-incidence spectrometer have been published before [2]. They were obtained by accumulating many consecutive pulses of our source. For the present investigations, we have devised a simpler low-resolution scheme that allows recording of the complete EUV spectrum by averaging only a few pulses or even by just using single pulses. Such data can be analyzed to obtain information on the achieved heating of the plasma and on the output stability in different wavelength regions.

The spectra were recorded using the transmission grating spectrometer arrangement shown in Figure 5. It consists of a Zr filter foil, a slit of 50 μm width, a gold transmission grating with 5000 lines/mm, and an EUV-sensitive back-illuminated CCD camera. In this setup, the spectral resolution was source-size limited to about $\Delta\lambda = 0.3$ nm. The data were corrected for the calculated wavelength dependence of the foil transmission and grating diffraction efficiency.

It was found that the spectral emission distribution depends strongly on the operating conditions. The distribution changes when the charging voltage, the current or the gas mixture or gas pressure are changed. The EUV spectra emitted from the plasma can be analyzed by comparison with model calculations in order to obtain information on the average ion stage distribution in the pinch under the different conditions. Figure 6 shows spectra of the DPF measured for single pulses at the same total gas pressure but for three different Xe flow rates. From analysis of relative intensity changes of the Xe IX to Xe XII line groups the average plasma temperature is seen to increase with decreasing Xe flow rate.

The stability of the single-pulse spectra is shown in Figure 7 for three pulses under similar operating conditions. The intensity fluctuations can be mainly attributed to differences of the final compression and heating of the pinch plasma from one pulse to the next. Generally, slightly larger fluctuations were observed for the regions on the short-wavelength side of the spectrum. They are dominated by the emissions of higher xenon ionization stages corresponding to the hottest regions of the pinch plasma.

The modeling included Hartree-Fock calculations with relativistic extensions and configuration interaction for the various xenon ions [5]. The dominant transitions are 4d –4f for the region around 11 nm and 4d – 5p from 12 to 17 nm. For the analysis, it is very advantageous that the latter transition arrays are fairly well separated for different ion stages Xe XII to Xe IX. As an approximation, we assumed a quasi-stationary plasma in thermal equilibrium and a Boltzmann distribution for the ion level populations. The opacity of the plasma is taken into account by weighting the transitions with an appropriate factor containing the oscillator strength explicitly. A comparison of higher resolution spectra with this calculation will be described in detail elsewhere [4]. Figure 8 shows the resulting spectrum for a particular ion stage distribution when folding with 0.2 eV or 1.9 eV, respectively. A comparison with the measured results of Figure 9 indicates that the main features of the experimental spectrum are reproduced apart from a broad background contribution that could originate from recombination continua.

5. ANGULAR STABILITY OF THE EUV OUTPUT ENERGY

The light from the DPF source will be collected at all azimuthal angles by grazing-incidence collection optics with large acceptance angle. Therefore, the angular stability of the emission from the source into different directions has to be examined. The dose stability and also the uniformity of the filling of the entrance pupil of the imaging optics are directly connected to this property.

The stability of the angular distribution of the EUV emission of our DPF light source is very high. This was confirmed by simultaneous measurements with two energy detectors. Figure 10 shows these detector arrangements that employ a foil and a multi-layer mirror for spectral filtering. The on-axis EUV emission was measured with a normal-incidence Mo/Si multi-layer mirror, a Zr foil and a photodiode (IRD AXUV-100). The off-axis EUV emission was recorded by EUV monitors on two sides consisting each of a multi-layer mirror with Mo/Si coating for 45 degree incident angle, a Zr foil and a photodiode. The EUV output energy was determined by time-integration of the photodiode signals. Differential pumping was achieved by means of apertures and turbo-molecular pumps.

High correlation of the in-band EUV emission was found when comparing the signals at different emission angles. In Figure 11, the measured average off-axis in-band output energy is plotted versus the corresponding on-axis output energy for DPF operation at low repetition rate using different input energies. The fit curve shows a direct proportionality with almost perfect correlation. As another example, Figure 12 shows the high pulse-to-pulse correlation obtained in a pulse train during burst-mode operation of the DPF at 2 kHz repetition rate using the two off-axis energy monitors. The correlation coefficient was 0.95 for these two data sets with 7% rms energy stability. Very high angular emission correlation was also observed for other detector combinations. These results indicate that for individual pulses the pinch dynamics leads to similar and highly correlated emission characteristics into different angular directions. Pulse averaging improves this correlation even further.

6. SOURCE IMAGING

The size of the source region for emission at 13.5 nm of the plasma pinch is a critical parameter for the design of an efficient light collection optics since the etendue directly influences the attainable collection efficiency [6,7]. Therefore, the source size should be matched to the collection optics and vice versa.

Previous measurements of the source size of our DPF were carried out at different viewing angles using pinhole-imaging techniques employing a spectral filtering foil, a pinhole and an EUV-sensitive CCD camera [2,3]. The results obtained by this technique can be limited by diffraction. Moreover, due to the use of the filter foil, normally radiation from a larger spectral region is sampled that does not exactly correspond to the radiation band selected by the 13.5 nm multi-layer mirrors of the imaging and projection optics.

Now, we have set up a new arrangement where no pinholes are used and the spectral filtering is mainly accomplished by multi-layer mirrors. This at-wavelength imaging method is illustrated schematically in Figure 13. Visible and UV light is suppressed by a Zr filter foil while in-band imaging and filtering is achieved by two spherical multi-layer mirrors in a 1:1 imaging configuration. In Figure 14, we show an on-axis source image obtained with this configuration for a 100 pulse average. Generally, it was found that the source sizes determined by this method gave slightly larger pinch diameters as compared to the imaging by the pinhole technique. The source position stability was also determined by this method. The fluctuations obtained for the centroid of these size measurements was typically less than 0.05 mm (rms).

7. DEBRIS MITIGATION

In order to minimize the generation of debris from plasma facing components it is necessary to understand the erosion rates of different materials subject to large pulsed heat loads. For any given power density and pulse duration, the temperature rise of the material is a function only of the thermal properties of the material [9]. For material erosion dominated by evaporation we can define a figure-of-merit called the impulsivity (M) [10] which is defined as:

$$M = T_m(\kappa\rho c)^{1/2} \quad (1)$$

where T_m is the melting point of the material, κ is the thermal conductivity, ρ is the mass density, and c is the specific heat at constant pressure. We have measured the erosion of several anode materials under similar conditions in our DPF dedicated to debris mitigation testing. Anodes of various materials were operated in the DPF at fixed dissipated energy, identical gas recipe, and for a known number of pulses. Anodes of the various materials were weighed before and after the testing. The materials tested included W, Cu, Al, Mo, stainless steel, and graphite. Figure 15 shows these materials listed in order of impulsivity with the corresponding erosion rate normalized to the tungsten electrode. All materials with the exception of graphite scale with the impulsivity. For these experiments graphite showed the highest erosion rate, although the impulsivity would suggest that a much better performance may be expected. The EUV output was also measured for these various electrodes. Comparable output powers were obtained for all anode materials, however, each anode exhibited a different optimum gas mixture for peak EUV power.

We have previously demonstrated [3] that the anode debris can be efficiently suppressed by use of a debris shield employing long channels. Such structures demonstrated stopping powers ~10^2/cm of channel length. In order to verify the stopping power of the channels and better understand the scaling of stopping power, we have constructed a multi-channel test fixture consisting of an array of channels of different lengths and angles relative to the pinch axis. This test fixture was mounted in front of the pinch on our DPF machine dedicated to debris mitigation.. A Si wafer witness sample was located immediately behind the test fixture. This arrangement, shown in Figure 16, was exposed for a fixed number of DPF pulses.

Examination of the Si wafer by several surface analytical techniques (XPS, Auger, and EDX) showed the presence only of C behind all of the open channels of the test fixture. Within the detection limits of these techniques no electrode material was seen within the C layer. No systematic scaling was observed for different channel lengths and entrance angles. These experiments were subsequently repeated on two additional DPF systems with similar results. From these experiments we may conclude that with the debris trap channels as shown in Figure 16 the rate of UV/EUV-catalyzed carbon deposition significantly exceeds the deposition rate of eroded electrode material. Base pressures of the three machines tested were ~10^{-6} Torr. A typical residual gas spectrum is shown in Figure 17. Efforts are now underway to remove all remaining sources of contamination in the system and repeat the experiments with an all-metal sealed system.

8. SUMMARY

A summary of the demonstrated source parameters is given in Figure 18. We have demonstrated consistent progress in improving the source output and conversion efficiency over the past few years. The conversion efficiencies with un-cooled electrodes are 0.45% at outputs of approximately 60 mJ/pulse. No fundamental problems exist for high-repetition rate operation at 4 kHz. CW operation at 1 kHz has validated our thermal designs for power extraction up to 13 kW.

Measurements of the angular stability of the EUV output energy show a high degree of correlation for EUV pulses emitted into different angles. This shows that variations in the angular emission characteristics of the source are not expected to have a significant impact on the dose stability. On-axis 1:1 imaging of the source has been performed using a multi-layer mirror. These measurements show that the source size measured in this way is slightly larger than that determined from pinhole images utilizing a Be or Zr filter foil. Typical sizes for our source are 0.38 mm FWHM.

We have demonstrated that a transmission grating spectrometer can be used to measure single-pulse spectra of the EUV source. This instrument can be used to tune the output of the source and determine in real-time the effects of adjusting the source parameters on the plasma temperature.

The erosion of the DPF anode as a function of the anode material was shown to scale with the impulsivity parameter which is a function of the specific material properties. Tungsten still remains the preferred choice for electrode material from the point of view of minimizing erosion, however, we have shown that

comparable EUV outputs can be obtained with a wide choice of electrode materials. We have re-confirmed that the multichannel debris shield concept can offer considerable stopping power for ejected electrode material. With the substantial reduction in debris arrival rate to our witness samples we now must address the issues of UV/EUV-catalyzed carbon deposition.

9. ACKNOWLEDGEMENTS

We would like to thank all of the technicians on the EUVL technology development team without whose help this work would not have been possible. In particular we would like to acknowledge Miguel Jaramillo, Terrance Houston, Vi Phung, and Richard Taddiken for their help on this project. We also extend our thanks to our excellent mechanical designer Ken LaValley who translated many of our ideas into workable designs.

10. REFERENCES

1. W. Partlo, I. Fomenkov, R. Oliver, D. Birx, "Development of an EUV (13.5 nm) Light Source Employing a Dense Plasma Focus in Lithium Vapor", in *Proc. of SPIE vol. 3997, Emerging Lithographic Technologies IV, ed. By E. A. Dobisz,* p. 136 (2000).
2. W. N. Partlo, I. V. Fomenkov, R. M. Ness, R. I. Oliver, S. T. Melnychuk, and J. E. Rauch, "Progress Toward Use of a Dense Plasma Focus as a Light Source for Production EUV Lithography", in *Proc. of SPIE vol. 4343, Emerging Lithographic Technologies V, ed. by E. A. Dobisz,* p. 232 (2001).
3. I. Fomenkov, W. Partlo, R.M. Ness, I. Oliver, S. T. Melnychuk, O. Khodykin, N. Böwering, "Optimization of a Dense Plasma Focus Device as a Light Source for EUV Lithography" in *Proc. of SPIE vol. 4688, Emerging Lithographic Technologies VI, ed. by R.L. Engelstad,* p. 634 (2002).
4. M. Martins, DESY, private communication
5. N. Böwering et al., to be published.
6. V. Banine, and R. Moors, "Extreme ultraviolet sources for lithography applications", *Proc. of SPIE vol. 4343, Emerging Lithographic Technologies V, ed. By E. A. Dobisz,* p. 203 (2001).
7. G. Derra and W. Singer, "Collection Efficiency of EUV Sources" this proceeding.
8. B. Bauer, et.al. this proceeding.
9. Handbook of Heat Transfer Fundamentals, 2nd edition, *ed. By W.M. Roshenow, J.P. Hartnett, and E.N. Ganic* McGraw-Hil*l* , New York, 1985, p. 4-108.
10. T. G. Engel, S. L. Wester, and M. Kristiansen, IEEE Trans. On Magnetics, **31(1),** 709 (1995).

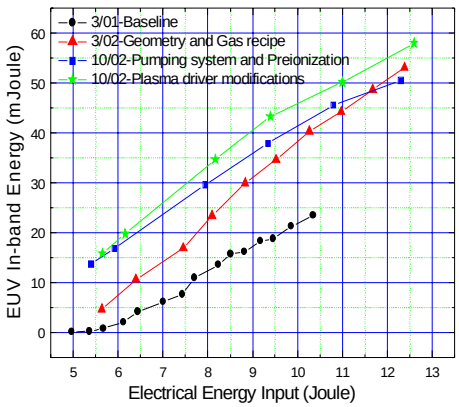

Figure 1. EUV In-band energy vs. Energy Input.

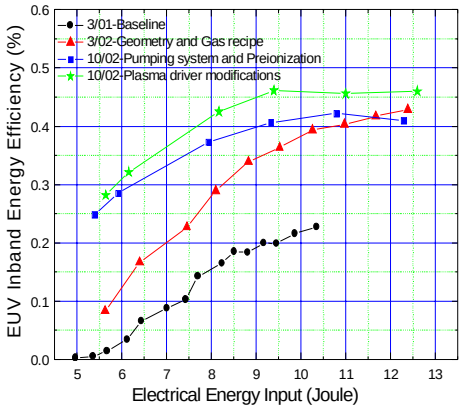

Figure 2. EUV In-band conversion efficiency vs. Energy Input.

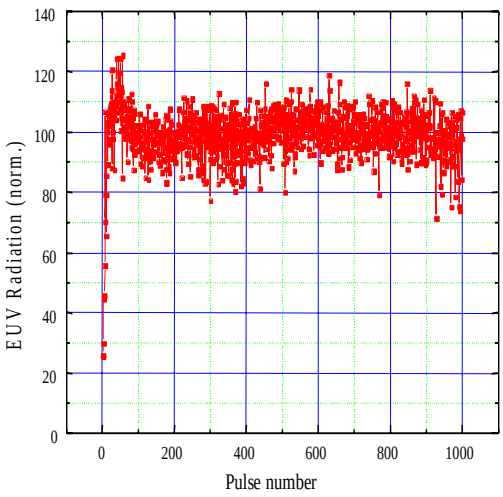

Figure 3. Normalized EUV In-band energy vs. Pulse Number. 2 kHz repetition rate; rms energy spread=7%.

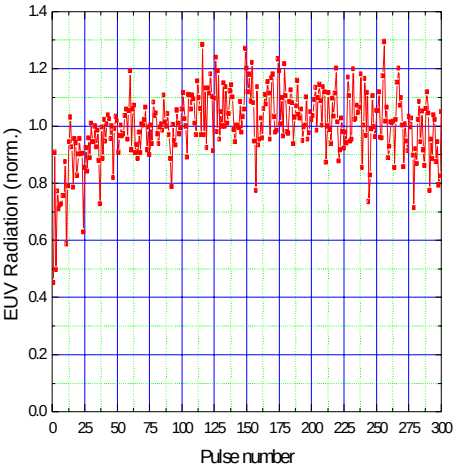

Figure 4. Normalized EUV In-band energy vs. Pulse Number. 4 kHz repetition rate; rms energy spread = 9%.

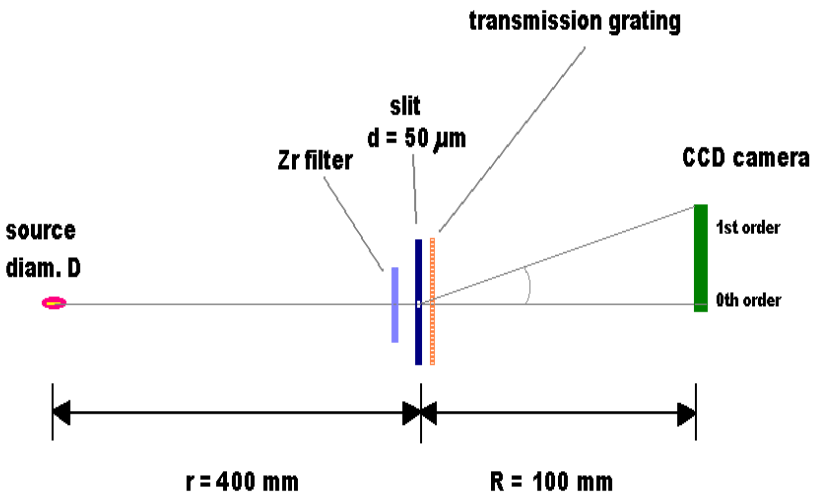

Figure 5. Schematic of the transmission grating spectrometer. 5000 lines/mm grating; resolution $\Delta\lambda$~0.3 nm.

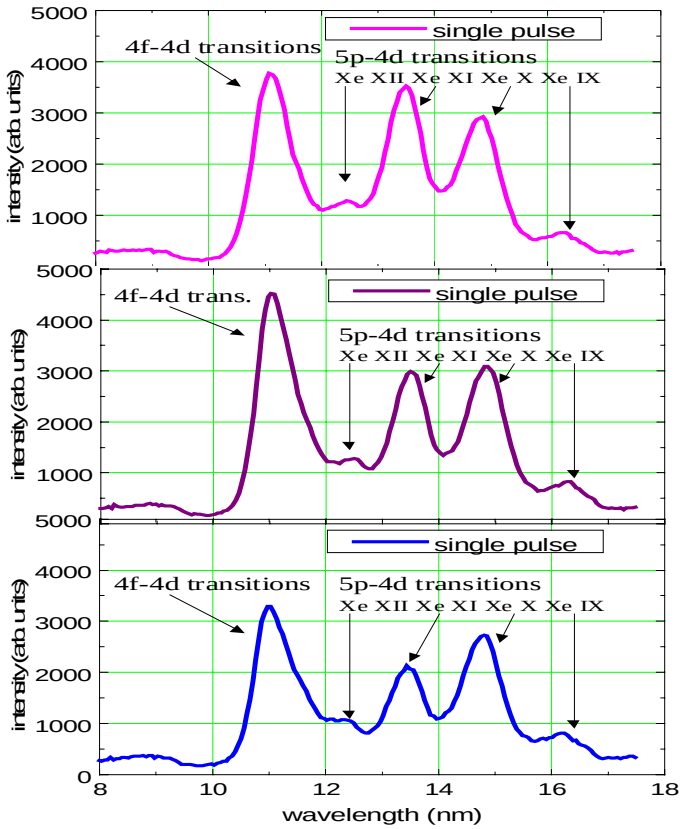

Figure 6. Single-pulse spectra at constant pressure vs. Xe flow rate. Xe flow rate increases from top to bottom. Plasma temperature decreases from top to bottom.

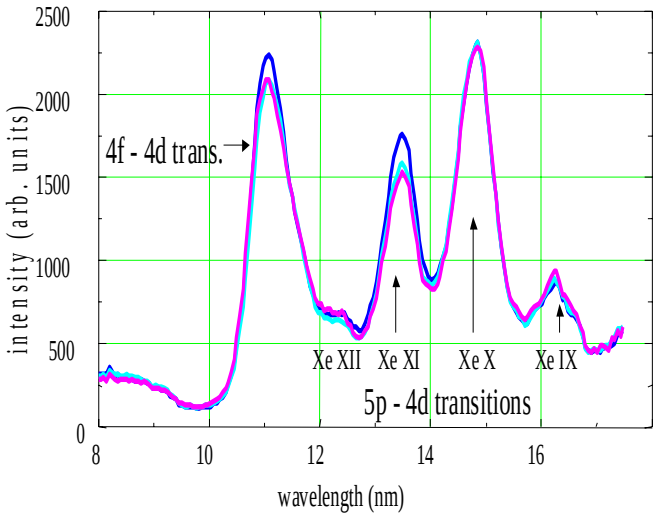

Figure 7. Single-pulse spectra at constant pressure and gas flow conditions.

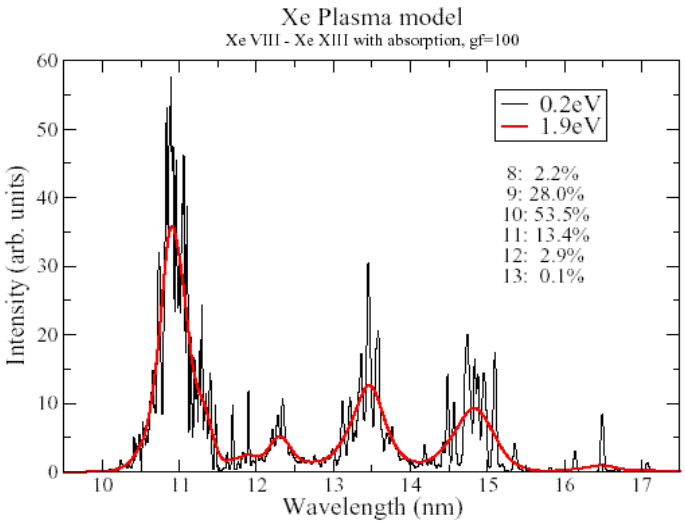

Figure 8. Calculated EUV spectra using the Hartree-Fock method. Black curve: 0.2 eV energy resolution; Red curve: 1.9 eV energy resolution. The table in the figure shows the fraction of Xe ion in the indicated charge state.

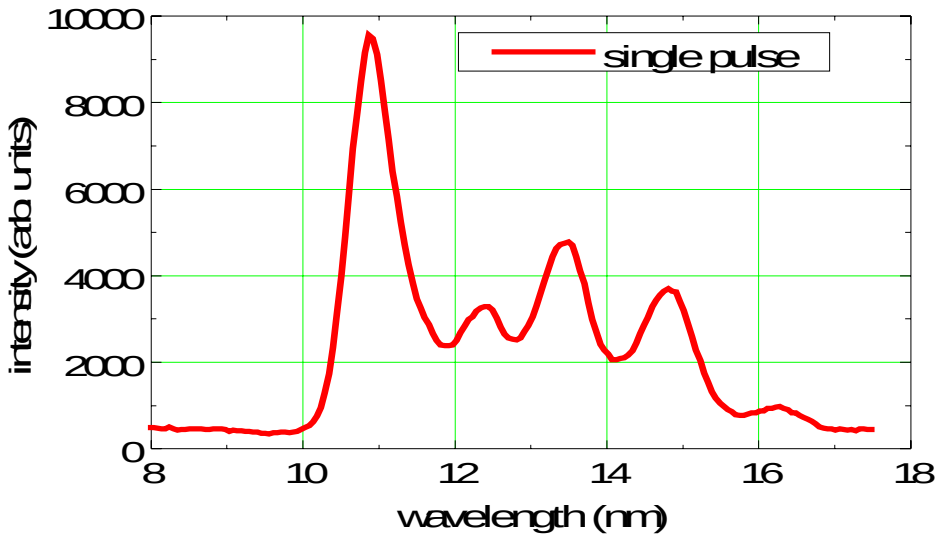

Figure 9. Single-pulse spectrum for comparison with calculated spectrum.

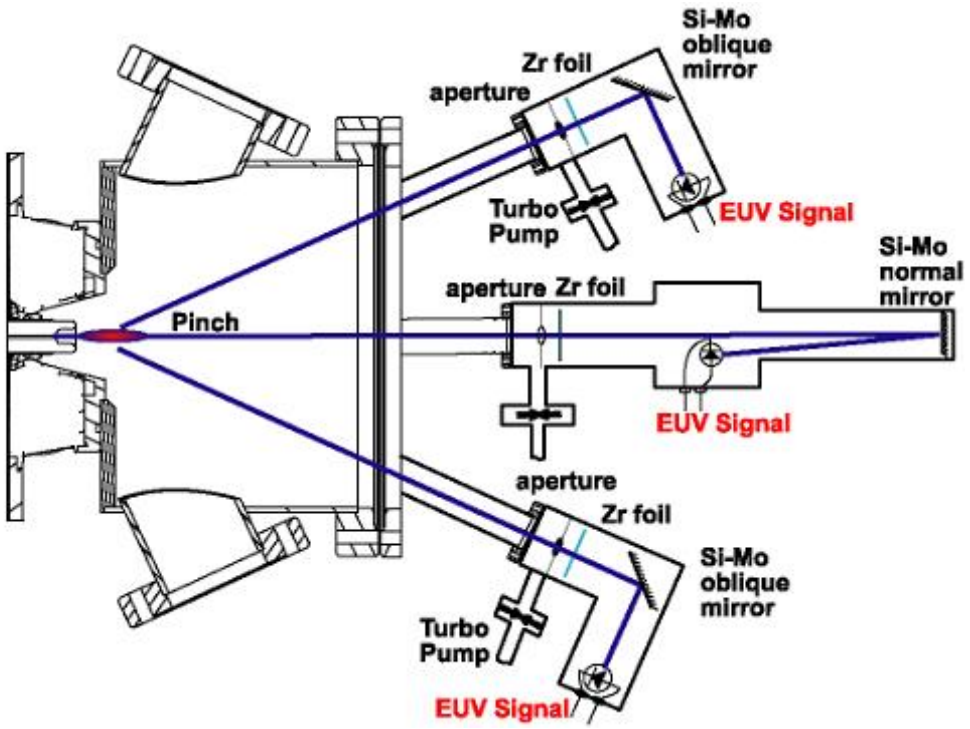

Figure 10. Experimental arrangement for measuring correlation of in-band EUV energy on and off-axis.

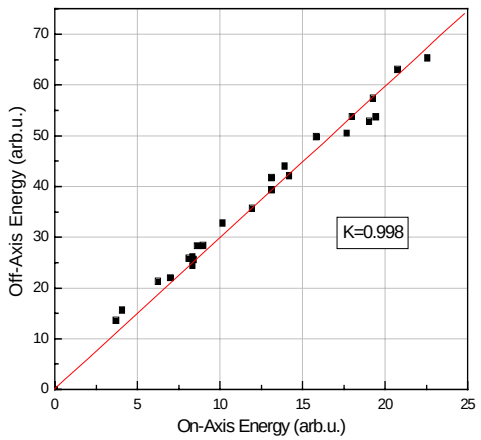

Figure 11. Off-axis EUV in-band energy vs. On-axis in-band EUV energy.

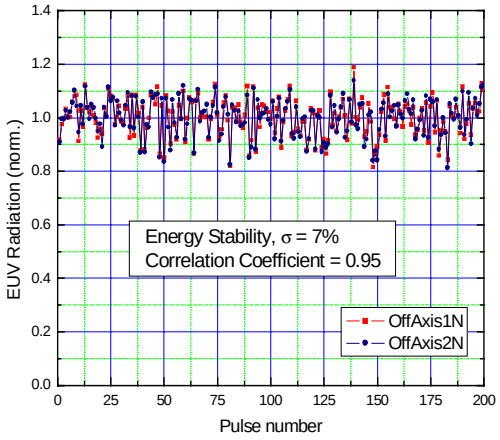

Figure 12. Correlation of two off-axis energy monitors vs. pulse number at 2 kHz repetition rate.

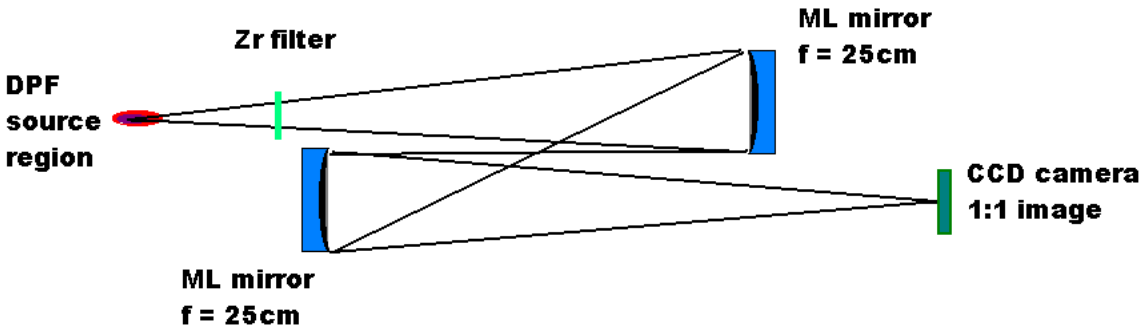

Figure 13. Experimental arrangement for 1:1 imaging of EUV source.

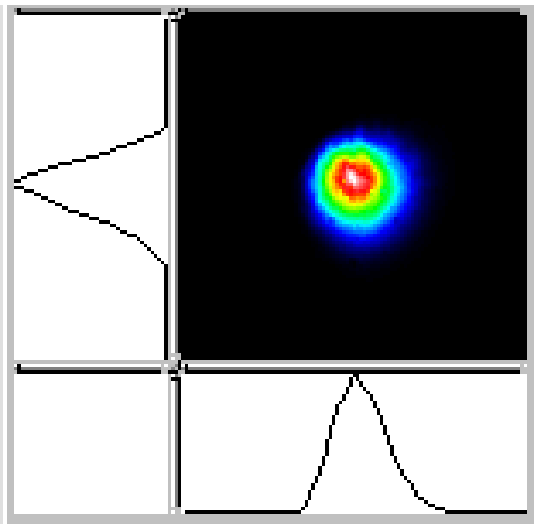

Figure 14. In-band EUV source image. FWHM = 0.38 mm.

Electrode material	Erosion rate	Impulsivity
	normalized	J/cm^2/sec^1/2
Tungsten	1	7000
Graphite	9	5700
Molybdenum	1.3	4800
Copper	2	4000
Stainless steel	3	1530
Aluminum	5.5	500

Figure 15. Measured erosion rate and Impulsivity parameter vs. Electrode material.

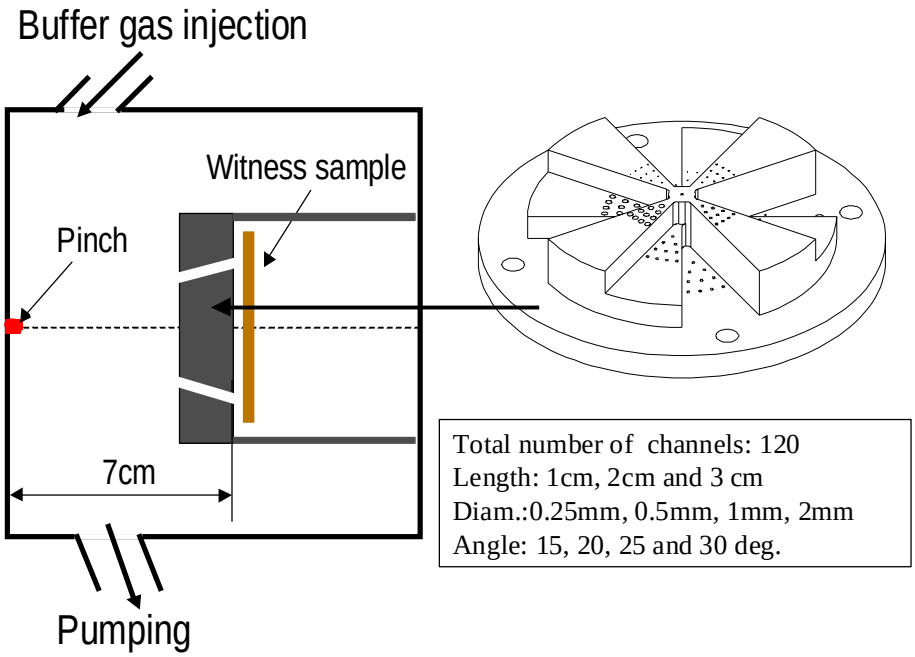

Figure 16. Experimental arrangement for measuring stopping power of long channels as a function of incident angle and channel length.

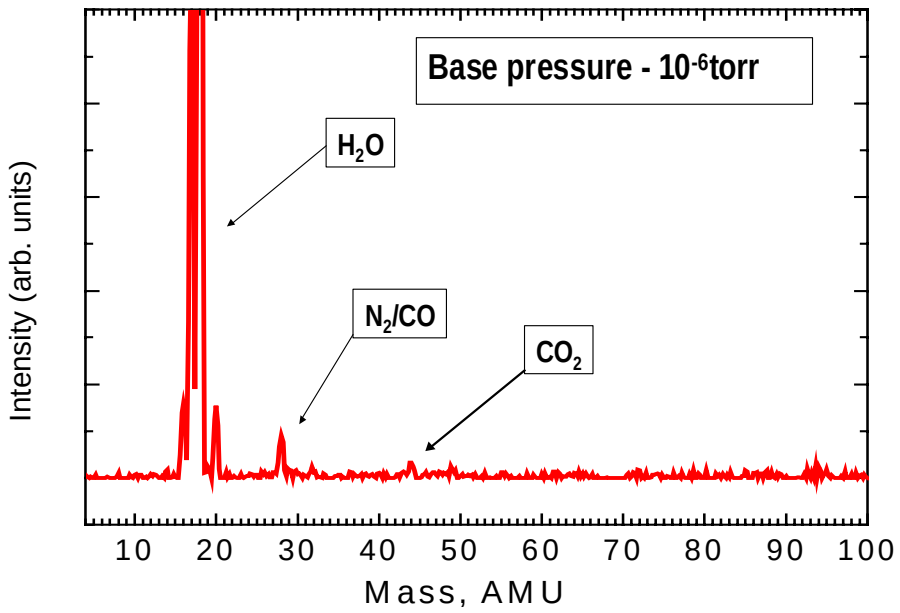

Figure 17. Residual gas spectrum of DPF vessel equipped with elastomer seals.

EUV efficiency with Xe, (2% BW, 2π sr)	> 0.45%
EUV energy per pulse (2% BW, 2π sr)	~ 55 mJ
Average source size (FWHM)	~ 0.4 x 2.5 mm
Source position stability (centroid)	< 0.05 mm, rms
Continuous repetition rate	1000 Hz
Burst repetition rate	4000 Hz
Energy Stability	~ 7 %, rms
Avg. EUV Output Power (2% BW, 2π sr)	50 Watt
EUV Output Power, Burst (2% BW, 2π sr)	200 Watt

Figure 18. Summary of DPF output performance.